Ovri, H.; Lilleodden, E.T.:

Temperature dependence of plastic instability in Al alloys: A nanoindentation study

In: Materials and Design (2017) Elsevier

DOI: 10.1016/j.matdes.2017.03.071

Temperature dependence of plastic instability in Al alloys: A nanoindentation study

Henry Ovri[1*], Erica T. Lilleodden[1,2]

[1]Helmholtz Zentrum Geesthacht, Institute of Materials Research, Materials Mechanics, 21502 Geesthacht, Germany.

[2]Technical University of Hamburg, Institute of Materials Physics and Technology, 21073, Hamburg, Germany.

Abstract

An elevated temperature nanoindentation based method for characterizing the thermal dependence of plastic instability and assessing the activation energies associated with the phenomenon in Al alloys is presented in this work. The method exploits the nanoscale force–displacement resolution capabilities of the Nanoindenter, precludes the ambiguities inherent in the uniaxial testing based methods and offers increased reliability because of the statistical significance of the data achieved. The activation energies estimated for an Al–Mg and an Al–Li alloy with the proposed method were found to be 0.59±0.07 eV and 0.72±0.01 eV, respectively, and are consistent with values derived with other methods. The rate controlling mechanisms associated with these activation energies are described in terms of existing models for plastic instability in these alloy systems.

Keywords: Aluminium alloys; nanoindentation; plastic instability; thermally activated processes

1 Introduction

The term plastic instability, as used in this work, refers to repetitive yielding that occurs in certain alloys during plastic deformation at critically low strain rates and over a range of temperatures, typically above room temperature. This phenomenon, otherwise known as Portevin-Le Chatelier (PLC) effect represents a material instability

that results in severe strain localization, reduction in ductility and formation of striations on the surfaces of sheet metals during forming processes. The combination of these deleterious effects with the environmentally induced embrittlement that may occur during service further accelerates the failure of the materials susceptible to PLC–type plastic instability [1]. This has implications for metal sheet forming applications, particularly in the automotive and aerospace industries where Al–based alloys, driven by their excellent strength-to-weight ratios, are becoming increasingly important.

Various aspects of PLC–type plastic instability, particularly the influence of strain rate [2][3], temperature [4][5] and precipitation [6][7][8][9] have been investigated. Such investigations form the basis for the development of mechanistic, theoretical and numerical models to explain the underlying microscopic mechanisms that govern plastic instability in solution strengthened and precipitation strengthened Al alloys. It is widely accepted that dynamic strain aging (DSA), i.e., the aging of both temporarily trapped mobile dislocations and forest dislocations by solutes with sufficient mobility, governs plastic instability in solution strengthened alloys [10]. It is argued that the negative strain rate sensitivity (nSRS) observed in alloy systems that exhibit plastic instability arises because the stress required to liberate the strain–aged mobile dislocations from the solute-decorated forest dislocation junctions is higher than that required to keep the mobile dislocations in motion upon their release [11][12]. The amount of solute that diffuses to the trapped mobile dislocations and, the associated 'break-free' stress are functions of the waiting time at the junctions between the trapped mobile dislocations and the dislocation forest. This in turn depends on the strain rate, temperature and the average dislocation density. The lower the strain rate, the longer the waiting time and the higher the 'break-free' stress. Conversely, higher temperature increases the solute diffusion rate and in turn leads to a higher 'break-free' stress [4][13]. While DSA

effectively describes the origin of plastic instability in solution strengthened Al–Mg base alloys, it has been shown that it cannot sufficiently account for the phenomenon in precipitation strengthened Al-Li based alloy systems [6][14][15]. A diffusion-controlled locking mechanism arising from the relaxation of the antiphase boundary of the ordered δ′ (Al_3Li) phase in Al–Li alloy systems during deformation at low strain rates was recently proposed as the mechanism governing PLC type plastic instability in Al–Li based alloys [6]. However, a quantitative treatment of the energetics required for such a mechanism has yet to be validated.

In order to gain further insights into the different rate controlling mechanisms in these two alloy systems, it is useful to probe the thermal dependence of the plastic instabilities. Such investigations provide insights into the local deformation mechanisms and facilitate the estimation of thermal activation parameters, such as activation volume and activation energy, associated with plastic instability. Different approaches [5][16][17] based on data from uniaxial tensile tests have been employed by various groups to arrive at these parameters. However, these approaches, as will be elaborated upon later, either have limited applicability, potential sources of error or are based on data lacking statistical significance. More so, the activation energies derived from these methods are usually less than those derived from theoretical and atomistic studies [11][13]. Yet it is not clear where the discrepancy lies.

In this work, we present an elevated temperature nanoindentation test method for characterising the thermal dependence of plastic instability and assessing the activation energy associated with the phenomenon in Al–Mg and Al–Li based alloys. Nanoindentation is particularly well suited for these kinds of investigations because of its high–resolution force–displacement capabilities, which makes it an effective tool for probing nanoscale perturbations such as plastic instability. This work demonstrates the

plausibility of the method, highlights the differences in plastic instability in these two alloy systems and extends upon the current state of mechanistic models for plastic instability more generally.

2 Materials and methods

Two aluminium alloys, a solid solution strengthened Al–Mg alloy, AA5182 and a precipitation strengthened Al–Li based alloy, AA2198, were used for this investigation. The Al–Mg based alloy had a nominal composition in wt.% of 4.5% Mg, 0.2–0.5% Mn, 0.35% Fe, 0.25% Zn, 0.15% Cu and 0.15% Cr. It was received and used in the annealed and rolled state. The Al–Li based alloy had a nominal composition in wt.% of 2.9–3.5% Cu, 0.8–1.1% Li, 0.25–0.8% Mg, 0.1–0.5% Ag, 0.04–0.18% Zr and 0.08% Si. This alloy was received in the naturally aged and stretched state and was then artificially aged at 370^{o}C for 10hours; a treatment which leads to an overaged temper state. A micrograph showing the key microstructural features obtained after this heat treatment is shown in Figure 1(a). The microstructure mainly consist of the metastable δ' (Al_3Li) precipitates, which has an $L1_2$ structure and is the main strengthening phase in this temper state, and equilibrium precipitates such as the T_2 (Al_5CuLi_3) and T_B (Al_7Cu_4Li) phases. Further details of the heat treatment protocol and the resulting microstructure are published elsewhere [19]. Samples from both alloys were prepared for the nanoindentation tests from the short-transverse direction of the rolled sheets and were then mechanically ground and polished prior to testing.

A ZHN Universal Nanomechanical hardness tester (Zwick/ASMEC) was used to conduct the nanoindention experiments. Unlike conventional nanoindentation systems, the force generation and force measurement systems in the ZHN nanoindenter are decoupled. The ability to record the force response in the material, in addition to the high force resolution (20nN) of this system, makes it possible to easily access the

nanoscale force perturbations arising from the plastic instabilities. Further advantages of the decoupled force generation and measurement system will be highlighted later. The ZHN nanoindenter is integrated with a laser heating system (Surface, GmBH) that can simultaneously heat up both the sample and indenter tip up to 500^{o}C. The laser heating system significantly minimises thermal drift by confining the heat to the sample and tip. The system additionally incorporates a water-cooled and temperature controlled system to ensure mechanical and thermal stability. The indentations made with the ZHN system were performed in a quasi–static, displacement controlled mode at a nominally constant strain rate of 0.003/s and at temperatures between 20 and 80^{o}C. The samples were held at each temperature for 30 minutes to ensure thermal stability and to prevent thermal gradients prior to testing. At least 15 indents were conducted for each test temperature, and all were made on a single sample of each alloy with a sapphire Berkovich indenter to a depth of 3um. The samples were re–tested at 20^{o}C upon completion of the elevated temperature tests in order to consider structural changes resultant from heating. In addition, a lamella for transmission electron microscopy (TEM) analysis was produced from the Al–Li alloy upon completion of the elevated temperature nanoindentation. The presence of the δ' phase, which is the main strengthening precipitate in this temper state, is still apparent as shown in Figure 1(b). The TEM lamella was produced by focused ion beam (FIB) milling in a Nova-200 dual beam scanning electron microscope, while it was examined in a Philips CM200 TEM operated at 200KV.

Due to the non–availability of the continuous stiffness measurement (CSM) capability in the ZHN system, it was not possible to compute the indentation hardness, H, in a straightforward manner since this requires the use of CSM to continuously assess the contact area, A. Conventionally, indentation hardness is given as [20]:

$$H = \frac{F}{A(h_c)}, \tag{1}$$

where F is the applied load and $A(h_c)$ is the area of the indent as a function of the contact depth, h_c. In the present work, the indenter tip area function was calibrated by manually fitting the imaged area of indents made to varying depths (between 0.5–4.0um) in a pure aluminium sample. The area function so derived was then used to compute the indentation hardness of the alloys as a function of indentation depth, h. Although this method of determining the area function of the indenter may lead to errors in absolute values of H, its use in this study do not affect subsequent analysis since mainly the difference in hardness, ΔH, is used.

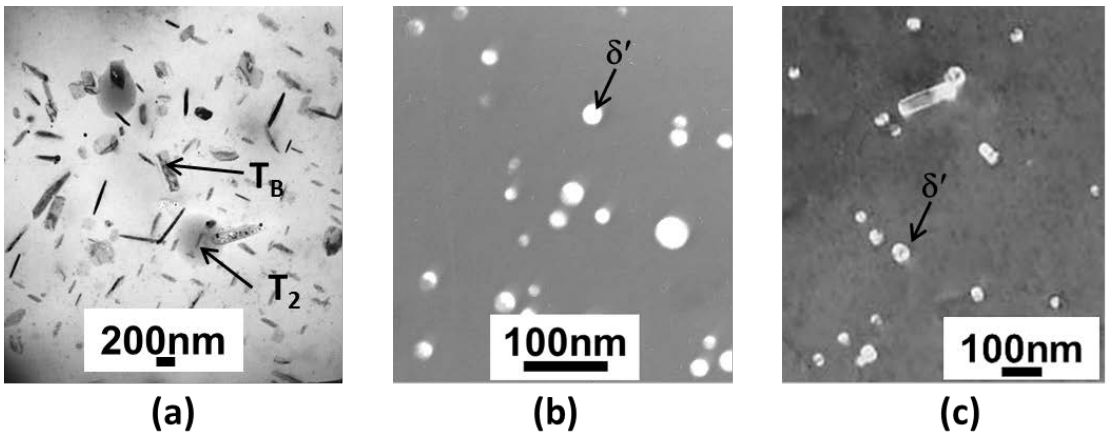

Figure 1: (a) Bright field and (b) Dark field images, showing the precipitates in the artificially aged Al–Li (AA2198) alloy prior to testing at elevated temperatures. Several precipitates including T_2 (Al_5CuLi_3), T_B (Al_7Cu_4Li) and the main strengthening phase, δ' (Al_3Li), are present in the grain interior of this temper state. (c) Dark field image of the alloy showing δ' phase after all tests at elevated temperatures. Fig. 1(a) and (b) are taken from [19] with permission.

3 Results and data analysis

The force–displacement response of the alloys at ambient temperature (20^{o}C) is shown in Figure 2(a). Both samples exhibit plastic instability at all test temperatures, with the instabilities manifesting as characteristic bursts in displacement. Each

displacement burst in Figure 2(b) macroscopically corresponds to an increase in the contact area of the indenter, and indicates a rapid release of mobile dislocations from obstacles where they have been temporarily locked. This behaviour is accompanied by a decrease in applied force to values lower than the resisting internal forces in the alloy. This decrease is subsequently followed by a steep rise in the applied force as the indenter tries to catch up with the material rapidly displaced from underneath the indenter during the displacement burst. We will refer to the local maximum force attained by the indenter prior to a displacement burst event as the "release" force, F_r. Likewise, we define a so–called arrest force, F_a, which is the force at the end of the displacement burst [21]. F_a is equivalent to the local force required to continue plastic deformation in the absence of the operation of the mechanism(s) that gives rise to plastic instability. Data points corresponding to F_r and F_a are highlighted in the insert in Figure 2(a). The displacement values, h_r and h_a, associated with F_r and F_a, respectively, are also highlighted in Figure 2(a). These data points were identified with an algorithm that determines local maxima and minima points in the displacement data and gives the corresponding time and force values. In order to prevent displacement burst events from being wrongly indexed, only indentation data beyond a displacement of 1um, where the steps are very well delineated and the noise in the signal is minimal, were considered.

Figure 2(c) shows the magnitude of the force difference, $\Delta F = F_r - F_a$, i.e. the force difference between consecutive displacement bursts, as a function of displacement. ΔF, rather than the magnitude of the displacement burst, $\Delta h = h_a - h_r$, was used in the analysis because the measured force signal, which is decoupled from the applied force, is expected to more accurately capture the material response than the displacement signal since the tests were conducted in displacement controlled mode. ΔF

and Δh scale linearly with displacement since the contact area of the Berkovich indenter scales with displacement. However, as a result of the self–similarity of the Berkovich indenter, the representative strain within the material is constant and independent of the applied force. This fact is highlighted in Figure 2(d) where the normalized difference in force, $\Delta F/F_r$, is plotted as a function of displacement. $\Delta F/F_r$ is roughly constant and independent of depth as expected for a geometrically self–similar indenter. It can be argued that statistical variations in the values of ΔF and $\Delta F/F_r$ arise from difference in the material response due to slight variations in the local microstructures of the alloys. It is also apparent from Figure 2 (c&d) that the magnitudes of ΔF and the corresponding, $\Delta F/F_r$ in the Al–Mg alloy are higher than those of the Al–Li alloy. This observed trend and the intermittent release and arrest of dislocations as described above clearly points to a material–dependent, local yield mechanism, which arises from thermally activated deformation processes. ΔF is equivalent to the break–free force and implicitly, the break–free stress associated with the mechanisms governing plastic instability while Δh is equivalent to the strain produced by ΔF. Consequently, we expect, in line with the mechanistic models for plastic instability highlighted earlier, that ΔF will be temperature and strain-rate dependent. We also note that the absolute value of ΔF will likely be influenced by the dynamics of the feedback system of the nanoindenter, as is the case for any instrument controlled with PID feedbacks. Moreover, the important parameter in the subsequent analysis is not necessarily the absolute value of ΔF but rather how ΔF scales with temperature. We expect that this trend is independent of dynamics of the instrument.

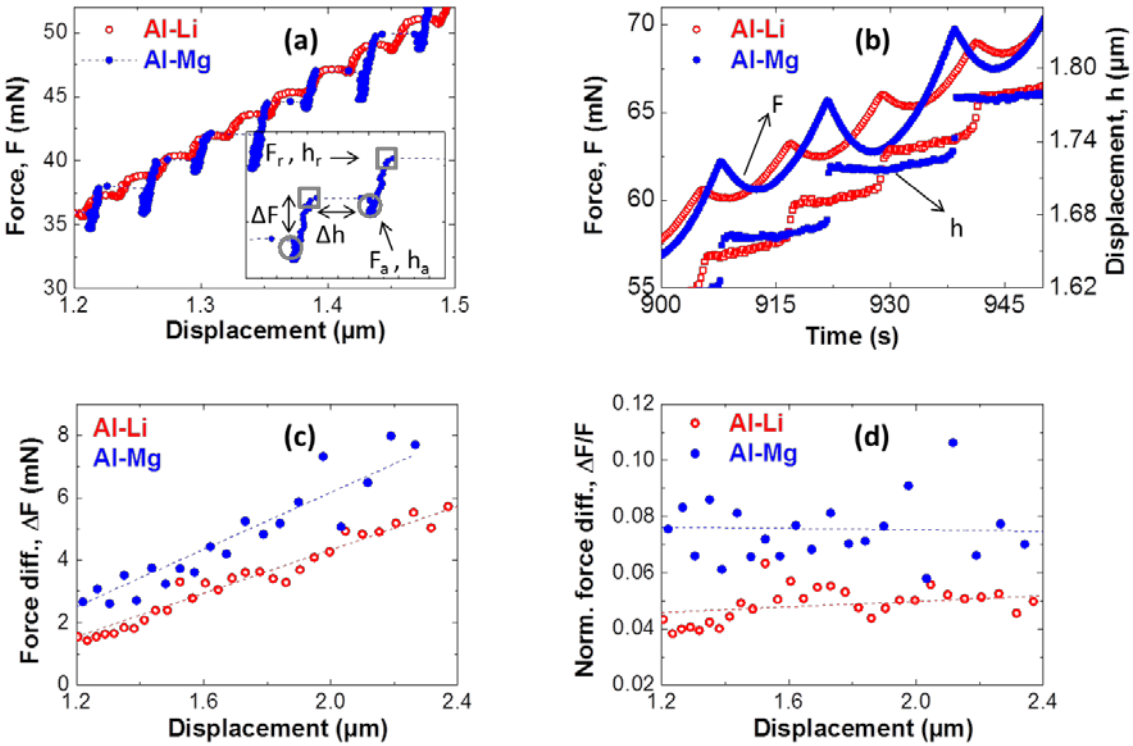

Figure 2: (a) Force–displacement response of both alloys (Al–Li in red open circles and Al–Mg in blue closed circles) at ambient temperature (20°C). Data points corresponding to the release force, F_r (in grey squares) and the arrest force, F_a (in grey circles), together with their corresponding the displacement values, h_r and h_a, respectively, are highlighted in the insert. (b) A plot of force and displacement for both alloys as a function of time. The decrease in force accompanying a displacement burst event is well captured by the indenter. (c) Shows the magnitude of the force difference, ΔF, between each F_r and the preceding F_a, as a function of displacement. ΔF increases linearly with displacement. (d) Shows the normalized difference in force, $\Delta F/F_r$, as a function of displacement. $\Delta F/F_r$ is roughly constant and independent of depth as expected for a geometrically self-similar indenter. The dashed lines in (c) and (d) are linear fits of the data points.

Figure 3 shows the force–displacement response of the Al–Li and Al–Mg samples at various temperatures. Although the characteristic steps indicative of plastic instability occur at all test temperatures in both alloys, the morphology of the steps in the Al–Li alloy is noticeably different from that of the Al–Mg alloy. Specifically, the magnitudes of the step size and the decrease in force accompanying the displacement burst in the Al–Li at all temperatures are smaller than those of the Al–Mg alloy. Another important difference is the high regularity of the characteristic steps in the Al–Li alloy as opposed to the less regular steps in the Al–Mg alloy. Moreover, smaller steps which were

unaccompanied by a drop in force where occasionally observed in the Al–Mg alloy at temperatures >20ºC. This behaviour is reminiscent of the A+B PLC deformation bands that are observed during tensile deformation of similar Al–Mg alloys at moderate strain rates [17]. Only the steps accompanied by a drop in force are considered in the present analysis.

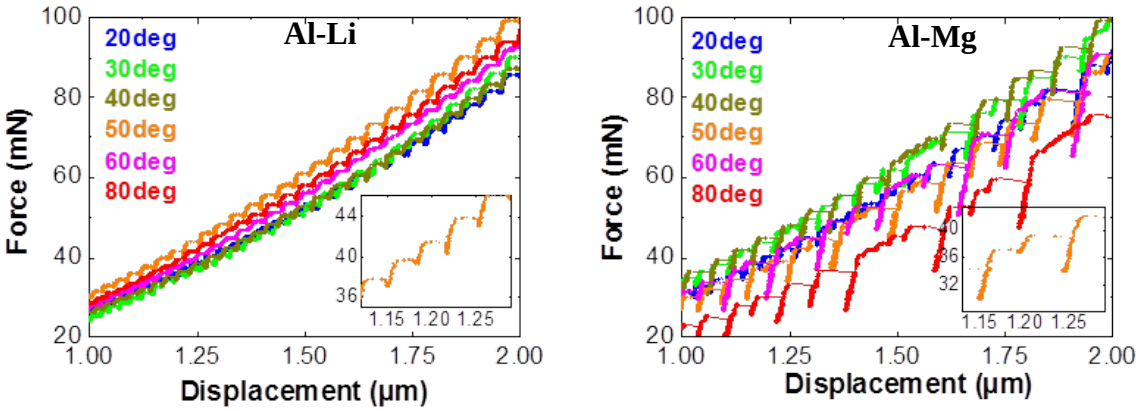

Figure 3: Force–displacement response of the Al–Li (left) and Al–Mg (right) alloys at various temperatures. Characteristic steps, indicative of plastic instability, are present at all test temperatures in both alloys.

In order to more effectively characterize the thermal dependence of the instabilities, we note that the hardness values at each F_r and F_a, i.e, H_r and H_a respectively, and consequently, the difference in hardness, ΔH, will also be temperature dependent.

$$\Delta H = H_r - H_a = \frac{F_r}{A(h_r)} - \frac{F_a}{A(h_a)}\,, \qquad (2)$$

where $A(h_r)$ and $A(h_a)$ are the projected areas of the indenter estimated from the displacements associated with each F_r and F_a, respectively. A plot of H_r and H_a at 20ºC is shown in Figure 4(a) as a function of displacement. The rather stochastic nature of the values of H_r and H_a as revealed by this plot, and consequently ΔH, necessitates the use of cumulative statistics to evaluate how temperature influences these properties. The cumulative distribution function (CDF) in particular has the advantage that it provides

an unbiased comparison of different sets of data as opposed to binning [23]. The CDF of the difference in hardness normalized by the elastic modulus, $\Delta H/E$, as a function of temperature is shown in Figure 4(b) for both alloys. The normalization was done with the room temperature modulus of the respective alloys since changes in the elastic modulus of Al alloys within the temperature range in which the tests were conducted are negligible [24]. We can argue that the curves are a good representation of the thermal dependence of ΔH because of the statistical significance of the data. Each of the curves in Figure 4(b) is an accumulation of all $\Delta H/E$ values (between 107 and 418 data points for the presented curves) from all 15 indentation tests at a given temperature. It is apparent from Figure 4(b) that the magnitude of $\Delta H/E$ increases with increase in testing temperature up to 50°C and 60°C for the Al-Li and Al-Mg alloy, respectively. A gradual decrease in $\Delta H/E$ was observed above these temperatures. The decrease in $\Delta H/E$ can be attributed to the operation of other deformation mechanisms, like dislocation cross slip and climb, which become more active at high temperatures. The competition between these mechanisms and those that govern plastic instability may lead to a suppression of the latter and consequently, a reduction of the magnitude of ΔH. It is also apparent from Figure 4(b) that the $\Delta H/E$ values for the Al–Mg alloy are significantly higher than those of the Al-Li alloy. Moreover, given the wider spread of the CDFs of the Al–Mg alloy in comparison to those of the Al–Li alloy, it can be argued that the effect of temperature on $\Delta H/E$ and, implicitly, on plastic instability is more pronounced in the Al–Mg alloy than in the latter. It was also observed that the CDFs of

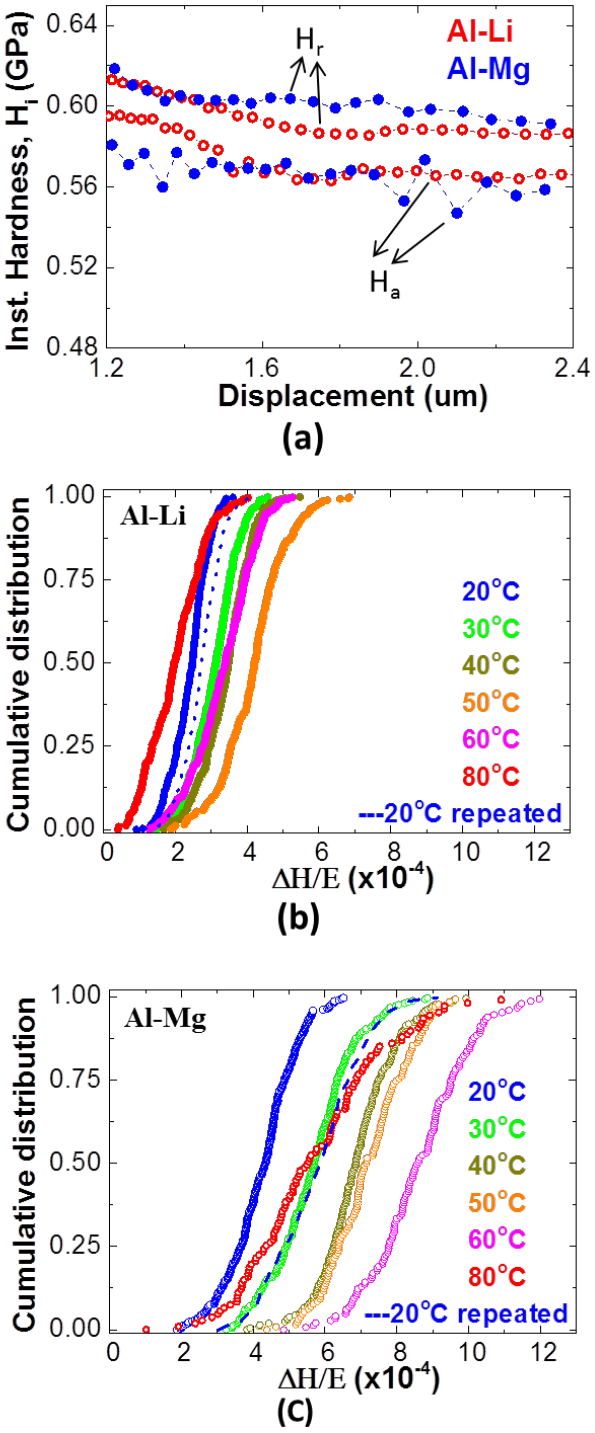

Figure 4: (a) A plot of instantaneous hardness at point of release and arrest, H_r (closed circles) and H_a (open circles), respectively, at 20°C is shown as a function of displacement for both Al-Li (in red) and the Al-Mg alloy (in blue). The hardness of both alloys is approximately the same but on close inspection ΔH (= $H_r - H_a$) appear large in the Al-Mg alloy than in Al-Li. Cumulative distribution function (CDF) of the modulus normalized difference in hardness, $\Delta H/E$, of the (b) Al-Li (closed circles) and (c) Al-Mg (open circles) alloys. The relatively larger values of $\Delta H/E$ and the wider spread of the CDFs of the Al-Mg alloy in comparison to that of the Al-Li alloy suggest that temperature has a more pronounced effect on plastic instability in the former.

the repeated 20°C tests, i.e. tests re-conducted on the samples at 20°C upon completion of all tests carried out at elevated temperatures, are shifted to the right of the CDFs of the initial 20°C tests. This suggests that slight changes must have occurred in the microstructures of both samples during testing at the elevated temperatures. It can however be argued that the effect is not significant, especially for the Al-Li alloy, since the curves of "repeated" 20°C tests are still very close to those of tests conducted at 30°C. Moreover, although not shown, it was observed that the mean hardness of the alloys as a function of temperature remained roughly within the scatter bands of all tests; a further indication that the temperatures at which the tests were conducted did not cause significant modification of the microstructures of the alloys.

The activation energy, ΔE, for plastic instability can be directly estimated from a plot of the mean values of $(\Delta H/E)$ vs test temperatures with the dislocation pile–up model proposed by Klose et. al. [25]. In the model, ΔE for plastic instability is evaluated from a plot of average stress drop, $\Delta\sigma$, vs temperatures, i.e., the temperature dependence of the difference in stress between the points of exhaustion of a dislocation avalanche and their subsequent breakaway from their pinned configurations, derived from constant strain rate uniaxial tensile tests. Since stress is proportional to hardness, and $\Delta\sigma$ is analogous to ΔH, the relationship proposed by these authors can be re–written as:

$$\frac{\Delta H}{E} \propto exp\left(-\frac{nq}{1-nq}\frac{\Delta E}{k_B T}\right), \tag{3}$$

where n is the diffusion or aging exponent, q is a constant that equals 1/2 for ideal dislocation pile ups at the obstacles during the aging process or 1 for single dislocations, K_B is the Boltzmann constant in eV/K and T is the test temperature in K. Following Klose et. al [5][25], we set $n = 1/3$ and $q = 1/2$. A plot of the mean values of

$ln\,\Delta H/E$ vs $1/T$ for both alloys, the slope of which gives ΔE, is shown in Figure 5. Only the slope of the data regime where $\Delta H/E$ increased with increase in temperature was used to estimate ΔE since the subsequent decrease in $\Delta H/E$ with increasing temperature is likely caused by the concurrent operation of other deformation mechanisms, such as were mentioned above.

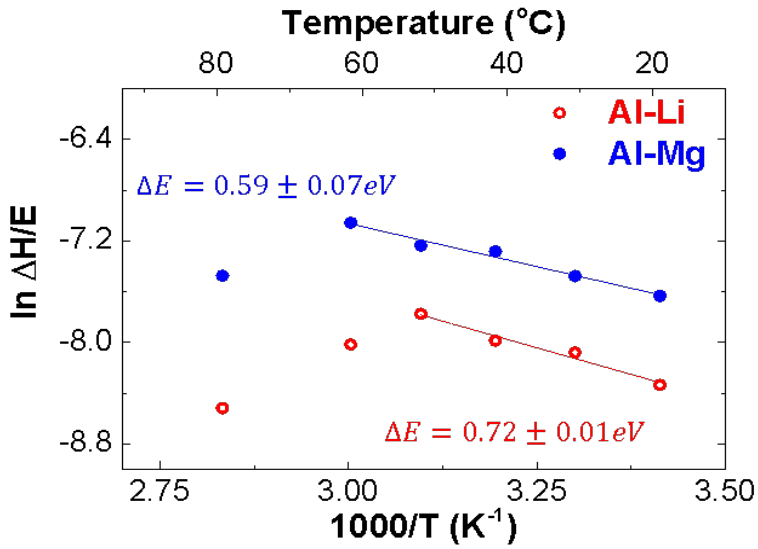

Figure 5: Temperature dependence of (ln) $\Delta H/E$ of the Al–Li (red open circle) and Al–Mg (blue closed circle) alloys. The activation energies, E_{app}, were estimated from the data regime where ln $\Delta H/E$ increased with increase in temperature.

4 Discussion

As mentioned earlier, various methods based on data from uniaxial tensile tests have been employed by other workers [5][16][17] to determine the activation energy for plastic instability. However, the conventional approach is based on the assumption that there is a critical strain, ε_c, for the initiation of plastic instability. The relationship between ε_c, strain rate, $\dot{\varepsilon}$, and temperature, T, is given as [26]:

$$\varepsilon_c{}^{m+B} = g'\dot{\varepsilon}\, exp\left(\frac{\Delta E}{RT}\right), \qquad (4)$$

where m and B are strain exponents, g' is a constant and R is the gas constant. The slope of a plot of $ln\,\dot{\varepsilon}$ vs. $ln\,\varepsilon_c$ gives the constants m and B, while ΔE is determined from the slope of $ln\,{\varepsilon_c}^{m+B}$ vs. $1/T$. Typical ΔE values reported for Al–Mg alloys using this approach are in the range of 0.48–0.65 eV [16][17][26] while values between 0.53–0.75 eV [27][28] have been reported for Al–Li alloys. It is remarkable that the ΔE values estimated for the Al-Mg and Al-Li alloy using the nanoindentation based approach, i.e. 0.59±0.07 eV and 0.72±0.01 eV, respectively, agree very well with ΔE values determined with the conventional approach. Nonetheless, the nanoindentation–based approach presented in this work has the advantage that it obviates potential errors inherent in the determination of ε_c. One such error arises from the fact that the apparent ε_c can be biased by the resolution of extensometer [6]. Furthermore, the conventional approach is limited to cases where there is an apparent ε_c, which is not always the case; a critical strain for the onset of plastic instability in the Al–Mg alloys is not always observed [4][17].

Klose et al [5] applied the same approach used in this work and obtained an ΔE for plastic instability of 0.6eV for an AA5182 alloy. Pink and Grinberg [17] reported an ΔE value of 0.52–0.67 eV for an Al–5%Mg alloy which they investigated. ΔE in this case was estimated from the slope of $log\left[\Delta\sigma(T/\Delta t)^{1.5}\right]$ vs. $1/T$, where $\Delta\sigma$ and Δt are the magnitude of the stress drop in a uniaxial tensile test and the time interval between consecutive stress drops, respectively. $\Delta\sigma$ was taken as the magnitude of the stress drop from its highest to its lowest point. The approach is based on the assumption that $\Delta\sigma$ scales with the amount of solutes that diffuse to temporarily trapped dislocations during deformation. These results agree very well with the results obtained for the same Al–Mg alloy investigated in this work with the nanoindentation method proposed herein.

The statistical significance of the method presented in this work however significantly increases its reliability in comparison to the method used in the other study.

The activation energy for plastic instability has also been estimated from the slopes of the boundaries of the onset and disappearance of plastic instability in a plot of $log\ \dot{\varepsilon}$ vs. $1/T$ [29]. This approach requires accurate knowledge of the strain rates, $\dot{\varepsilon}$, at which plastic instability appears and disappears at various temperatures, T. The inherent difficulty in determining ΔE from this method may explain the rather wide range of ΔE, 0.86–1.09 eV [4], 0.46–0.64 eV [17] and 0.3±0.1 eV [29] obtained for similar Al-Mg alloys by various authors. It is worth noting that the ΔE values obtained in this work agree well with those reported by several other workers [5][16][17][26][27][28] with the exception of Refs. [4] and [29].

Although there is good agreement between the ΔE values obtained in this work and those obtained with other methods, the ΔE values are significantly lower than the activation energies values for bulk diffusion, ΔE_{bulk}, of Mg in Al, ~1.20 eV [4] and that of Li in Al, ~1.35 eV [28]. This supports the already established fact that bulk diffusion of these solute species to dislocations temporarily trapped at obstacles does not govern plastic instability in these alloy systems. These values are also significantly lower than the activation energy for cross-core diffusion, ΔE_c, of Mg in Al, ~0.97 eV, obtained from atomistics [11]. Cross-core diffusion, i.e., the single atomic jumps of solute species from the compression to the tension side of the slip plane within the dislocation core, was recently proposed as the rate controlling mechanism for plastic instability in Al–Mg alloys [30]. Atomistic studies by Picu and Zhang [13] also indicate that the activation energy for pipe diffusion, ΔE_p, of Mg in Al, i.e. diffusion of solutes from solute clustered forest dislocations to unclustered mobile dislocations along their dislocation cores, without the assistance of extrinsic vacancies is >1.0 eV. Interestingly,

the simulations also show that the value of ΔE_p decreases to 0.61 eV in the presence of sufficient concentration of vacancies. This value is on the same order as obtained in experiments and may be an indication that pipe diffusion of some sort in the presence of vacancies may be the rate controlling mechanism governing plastic instability in Al–Mg alloys. However, it is not certain whether sufficient vacancies, introduced either during prior processing and/or during deformation, are present to drive pipe diffusion in these alloy systems.

We previously showed that strain aging by Li atoms does not govern plastic instability in precipitation strengthened Al–Li alloys [6]. In other words, the ΔE obtained in this work, 0.72±0.01 eV, is associated with a rate controlling mechanism other than the vacancy-assisted pipe diffusion of Li. The main thrust of the diffusion-controlled locking mechanism, which was proposed as the governing mechanism for plastic instability in Al–Li based alloys, is that the energy of the antiphase boundary (APB) formed in the active glide plane of the ordered δ' phase upon shearing by the leading superpartial dislocation is sufficiently lowered by local atomic rearrangements within the APB during deformation at low strain rates. We argued that the atomic rearrangements are driven by the need to reduce the number of like–bonds across the APB interface. The subsequent relaxation of the APB leads to the locking of the trailing superpartial dislocation and consequently an increase in applied stress. Negative strain rate sensitivity (nSRS) is a natural consequence of this mechanism since the magnitude of the increase in applied stress decreases with increase in strain rate or with decrease in temperature [6]. Although it is outside the scope of this work to determine the theoretical activation energies associated with the pseudo–locking mechanism, we argue that there is sufficient evidence in the literature showing that such a mechanism occurs in the presence of ordered phases. Sanchez and co–workers [31] modelled the

equilibrium structures of APBs in $L1_2$–ordered phases using the cluster variation method; they showed that the APB becomes more diffuse, inducing disorder on several adjacent planes as temperature is increased or strain rate is lowered. They also showed that the thickness of the diffuse APB is exacerbated by a slight deviation from the stoichiometry of the $L1_2$ phase or micro–segregation of one of the alloy components to the APB. The model is further supported by Schoeck [32] and Morris [33], who studied the kinetics of the APB relaxation process. Morris argued that the relaxation rates in $L1_2$ ordered Al_5Ti_2X systems in the other of 10^{-2}–10^{-3}/s can be expected at 0.5–0.7 T/T_c, where T_c is the critical order–disorder temperature, and that the relaxations can reduce the APB energy by over 50%. The fast relaxation rates and the magnitude of the decrease in APB energy accompanying the relaxation of APB suggest that the activation energies associated with the mechanism will be rather low and may be in the region of the activation energy obtained experimentally.

5 Concluding remarks

A novel nanoindentation–based method has been successfully implemented to study the thermal dependence of plastic instability in two distinct Al alloys: the Al–Mg solute strengthened alloy, AA5182 and the precipitation strengthened Al–Li alloy, AA2198. We were able to determine the apparent activation energies, ΔE, associated with the phenomenon for each system, and considered them in light of current models of rate controlling mechanisms. We showed that the magnitude of the difference in hardness between consecutive displacement burst events, ΔH, is material dependent and also a function of temperature. A plot of the cumulative distribution of the difference in hardness, normalized by the elastic modulus, $\Delta H/E$, clearly revealed the influence of these variables on plastic instability; these influences are ordinarily hidden by the stochastic nature of the displacement burst events. The ΔE associated with plastic

instability in both alloys was also directly estimated from the mean values of $\Delta H/E$ at the different test temperatures using a slightly modified modulus compensated hot hardness relationship. While the ΔE values obtained for both alloys with the method proposed in this work are in good agreement with ΔE obtained with uniaxial tests based methods, we argue that the former offers improved reliability and obviates potential sources of errors inherent in the latter.

6 References

[1] A. Yilmaz, The Portevin-Le Chatelier effect: a review of experimental findings, Sci. Tech. of Adv. Mater. 12 (2011) 063001.

[2] H. Dierke, F. Krawehl, S. Graff, S. Forest, J. Sachl, H. Neuhäuser, Portevin-Le Chatelier effect in Al-Mg alloys: Influence of obstacles – experiments and modelling, Comp. Mater. Sci. 39 (2007) 106–112.

[3] G.J. Fan, G.Y. Wang, H. Choo, P.K Liaw, Y.S. Park, B.Q. Han, E.J. Lavernia, Deformation behaviour of an ultrafine-grained Al-Mg alloy at different strain rates, Scr. Mater. 52 (2005) 929–933.

[4] R.C. Picu, G. Vincze, F. Ozturk, J.J. Gracio, F. Barlat, A.M. Maniatty, Strain rate sensitivity of the commercial aluminium alloy AA5182–O, Mater. Sci. & Eng. A 390 (2005) 334–343.

[5] F.B. Klose, A. Ziegenbein, F. Hagemann, H. Neuhäuser, P. Hähner, M. Abbadi, A. Zeghloul, Analysis of Portvein-Le Chatelier serrations of type B in Al–Mg, Mater. Sci. & Eng. A 369 (2004) 76–81.

[6] H. Ovri, E.T. Lilleoden, New insights into plastic instability in precipitation strengthened Al-Li alloys, Acta Mater. 89 (2015) 88–97.

[7] P.J. Gregson, D.S. McDarmaid, E. Hunt, Post-yield deformation characteristics in Al-Li alloys, Mater. Sci. & Tech. 4 (1988) 713–718.

[8] A. Deschamps, B. Decreus, F. De Geuser, T. Dorin, M. Weyland, The influence of precipitation on plastic deformation of Al–Cu–Li alloys, Acta Mater. 61 (2013) 4010–4021.

[9] Tian B. B. Tian, Comparing characteristics of serrations in Al–Li and Al–Mg alloys, Mater. Sci. & Eng. A 360 (2003) 330–338.

[10] Min J, Hector Jr. LG, Carsley JE, Stoughton TB, Carlson BE, Lin J. Spatio-temporal characteristics of plastic instability in AA5182-O during biaxial deformation. Mater. & Des. 83 (2195) 786-794.

[11] M.A. Soare, W.A Curtin, Solute strengthening of both mobile and forest dislocations: the origin of dynamic strain aging in FCC metals, Acta Mater. 56 (2008) 4046–4061.

[12] E. Rizzi, P. Hähner, On the Portevin–Le Chatelier effect: theoretical modelling and numerical results, Intl. J. of Plast. 20 (2004) 121–165.

[13] R.C. Picu, D. Zhang, Atomistic study of pipe diffusion in Al–Mg alloys, Acta Mater. 52 (2004) 161–171.

[14] E. Pink, S. Kumar, T. Baohui, Serrated flow of aluminium alloys influenced by precipitates, Mater. Sci. & Eng. A 280 (2000) 17–24.

[15] N. Behnood, J.T. Evans, Plastic deformation and the flow stress of aluminium lithium alloys, Acta Metall. 37 (1989) 687–695.

[16] K. Peng, W. Chen, K. Qian, Study on dynamic strain aging phenomenon of 3004 aluminium alloy, Mater. Sci. Eng. A 415 (2006) 53–58.

[17] E. Pink, A. Grinberg, Stress drops in serrated flow curves of Al5Mg, Acta Metall. 30 (1982) 2153–2160.

[18] A, Kalk, C, Schwink, On dynamic strain ageing and the boundaries of stable plastic deformation studied on Cu-Mn polycrystals, Phil. Mag. A 72 (1995) 315–339.

[19] H. Ovri, E.A. Jägle, A. Stark, E.T. Lilleodden, Microstructural influences in a naturally aged and overaged Al-Cu-Li-Mg based alloy, Mater. Sci. & Eng. A 637 (2015) 162–169.

[20] W.C. Oliver, G.M. Pharr, An improved technique for determining hardness and elastic modulus using load and displacement sensing indentation experiments, J. Mater. Res. 7 (1992) 1564–1583.

[21] M.J. Cordill, N.R. Moody, W.W. Gerberich, The role of dislocation walls for nanoindentation to shallow depths, Intl. J. Plast. 25 (2009) 281–301.

[22] C.A. Schuh, T.G. Nieh, A nanoindentation study of serrated flow in bulk metallic, Acta Mater 51 (2003) 87–99.

[23] J.K. Mason, A.C. Lund, C.A. Schuh, Determining the activation energy and volume for the onset of plasticity during nanoindentation, Phys. Rev. B 73 (2006) 054102.

[24] A. Alankar, M.A. Wells, Constitutive behaviour of as-cast aluminium alloys AA3104, AA5182 and AA6111 at below solidus temperatures, Mater. Sci. & Eng. A 527 (2010) 7812–7820.

[25] F.B. Klose, J. Weidenmüller, A. Ziegenbein, P. Hähner, H. Neuhäuser, Plastic instabilities with propagating deformation bands in Cu–Al alloys, Phil. Mag. 84 (2004) 467–480.

[26] A. Asgharzadeh, H.J. Aval, S. Serajzadeh, A study on flow behaviour of AA5086 over a wide range of temperatures, J. Mater. Eng. Perf. 25 (2016) 1076–1084.

[27] S. Kumar, E. Pink, Serrated flow in aluminium alloys containing lithium, Acta Mater. 45 (1997) 5295–5301.

[28] J.C. Huang, G.T. Gray, Serrated flow and negative rate sensitivity in Al-Li based alloys, Scri. Metall. et Mater. 24 (1990) 85–90.

[29] M. Abbadi, P. Hähner, A. Zeghloul, On the characteristics of Portevin-Le Chatelier bands in aluminium alloy 5182 under stress-controlled and strain-controlled tensile testing, Mater. Sci. & Eng.A 337 (2002) 194–201.

[30] Curtin W.A. Curtin, D.L. Olmsted, L.G .Hector, A predictive mechanism for dynamic strain ageing in aluminium–magnesium alloys Nat. Mater. 5 (2006) 875–880.

[31] J.M. Sanchez, S. Eng, Y.P. Wu, J.K. Tien, Modelling of antiphase boundaries in L12 structures, Mater. Res. Soc. Symp. Proc. 81 (1987) 57–64.

[32] G. Schoeck, A. Korner, The temperature dependence of the antiphase boundary energy in Ni3Fe II. The evolution kinetics, Phil. Mag. A 61 (1990) 917–928.

[33] D.G. Morris, Grown-in and shear-produced APB faults in ordered intermetallics, in: C.T. Liu, R.W. Cahn, G. Sauthoff (Eds), Ordered intermetallics – Physical metallurgy and mechanical behaviour, Kluwer Academic Publishers, Dordrecht, 1992, pp. 123–142.